8134 *Inorg. Chem.* **2009**, *48*, 8134–8144
DOI: 10.1021/ic900208a

Inorganic Chemistry
Article

Three-Coordinate, Phosphine-Ligated Azadipyrromethene Complexes of Univalent Group 11 Metals

Thomas S. Teets,[†] James B. Updegraff III,[†] Arthur J. Esswein,[‡] and Thomas G. Gray*[,†]

[†]*Department of Chemistry, Case Western Reserve University, Cleveland, Ohio 44106, and* [‡]*Department of Chemistry, Massachusetts Institute of Technology, Cambridge, Massachusetts 02139*

Received February 2, 2009

Tetraarylazadipyrromethenes are Lewis basic, red-light absorbing dyes with optical properties conducive to sensing and therapeutic applications. Recently, transition metal complexes of these ligands have been described. Here, we report a series of three-coordinate Group 11 complexes of unsubstituted and methoxy-substituted tetraarylazadipyrromethenes. In each, two pyrrole nitrogens chelate a d^{10} metal ion; triphenyl- or triethylphosphine occupies a third coordination site. New complexes are characterized by multinuclear NMR, X-ray crystallography, optical absorption and emission spectroscopy, and elemental analysis. Solid-state structures show trigonal planar geometries about the metal centers, and reveal pervasive intra- and intermolecular π-stacking interactions. Visible light absorption intensifies with metal binding, in some cases shifting to longer wavelengths. The complexes weakly luminesce in the red region; emission wavelengths and quantum yields are similar to those of free azadipyrromethenes. Methoxy-substitution on the ligand red-shifts optical features, whereas substitution of triethylphosphine for triphenylphosphine in the third coordination site has minimal structural or spectral consequences.

Introduction

Dipyrromethenes and azadipyrromethenes are chromophoric, bidentate Lewis bases of great importance because of their boron adducts. Scheme 1 depicts the general structures of dipyrromethene and azadipyrromethene BF_2^+ chelates. Boron dipyrromethenes and azadipyrromethenes absorb visible light and yield intense fluorescence; their optical attributes prompt continuing scrutiny.

Difluoroboron dipyrromethenes are marketed as BODIPY dyes.[1] These absorb light at a range of frequencies (ca. 500−650 nm in methanol) depending on peripheral substitution. Stokes shifts are small, and an emission spectrum that mirrors the principal absorption band reaches a maximum at wavelengths 10−20 nm red-shifted from the absorption peak. Emission persists with 4 ns or longer lifetimes, and fluorescence quantum yields often exceed 80%. The BODIPY chromophore is non-ionizable, and optical characteristics are minimally sensitive to pH or solvent polarity. Substitution is possible through the pyrrolic carbon atoms, at the backbone methine carbon, or along phenyl substituents at the methine carbon. Much current research explores substitution at boron, in some cases with moieties that themselves fluoresce.[2−4] Applications to bioconjugate chemistry are legion, not least because of the chromophores' wide optical tunability. Remote functionalization through a backbone phenyl ring (at C-5, Scheme 1a) allows chemical attachment with minimal changes in optical properties. Reports of nucleotide, protein, and lipid tagging with these versatile fluorophores are now common.[5−20]

*To whom correspondence should be addressed. E-mail: tgray@case.edu.

(1) BODIPY is a registered trademark of Molecular Probes, Inc.

(2) Ulrich, G.; Goze, C.; Guardigli, M.; Roda, A.; Ziessel, R. *Angew. Chem., Int. Ed.* **2005**, *44*, 3694–3698.
(3) Goze, C.; Ulrich, G.; Mallon, L. J.; Allen, B. D.; Harriman, A.; Ziessel, R. *J. Am. Chem. Soc.* **2006**, *128*, 10231–10239.
(4) Ziessel, R.; Goze, C.; Ulrich, G.; Césario, M.; Retailleau, P.; Harriman, A.; Rostron, J. P. *Chem.—Eur. J.* **2005**, *11*, 7366–7378.
(5) Chang, T.-C.; Lin, J.-J.; Lin, K.-C.; Lin, Y.-C.; Huang, W.-C.; Yang, Y.-P.; Cheng, J.-Y. *J. Lumin.* **2002**, *98*, 149–152.
(6) Gite, S.; Mamaev, S.; Olejnik, J.; Rothschild, K. *Anal. Biochem.* **2000**, *279*, 218–225.
(7) Epand, R. F.; Sayer, B. G.; Epand, R. *FEBS J.* **2005**, *272*, 1792–1803.
(8) Teske, C. A.; Schroeder, M.; Simon, R.; Hubbuch, J. J. *J. Phys. Chem. B* **2005**, *109*, 13811–13817.
(9) Fernandes, F.; Loura, L. M. S.; Prieto, M.; Koehorst, R.; Spruijt, R. B.; Hemminga, M. A. *Biophys. J.* **2003**, *85*, 2430–2441.
(10) Sculimbrene, B.; Imperiali, B. *J. Am. Chem. Soc.* **2006**, *128*, 7346–7352.
(11) Coleman, M. A.; Lao, V. H.; Segelke, B. W.; Beernink, P. T. *J. Proteome Res.* **2004**, *3*, 1024–1032.
(12) Janosch, S.; Nicolini, C.; Ludolph, B.; Peters, C.; Völkert, M.; Hazlet, T. L.; Waldmann, H.; Winter, R. *J. Am. Chem. Soc.* **2004**, *126*, 7496–7503.
(13) Krüger, P.; Baatz, J. E.; Dluhy, R. A.; Lösche, M. *Biophys. Chem.* **2002**, *99*, 209–228.
(14) Reaven, E.; Leers-Sucheta, S.; Nomoto, A.; Azhar, S. *Proc. Natl. Acad. Sci. U.S.A.* **2001**, *98*, 1613–1618.
(15) Bergström, F.; Hägglöf, P.; Karolin, J.; Ny, T.; Johansson, L. B.-Å. *Proc. Natl. Acad. Sci. U.S.A.* **1999**, *96*, 12477–12481.
(16) Yee, M.-c.; Fas, S. C.; Stohlmeyer, M. M.; Wandless, T. J.; Cimprich, K. A. *J. Biol. Chem.* **2005**, *280*, 29053–29059.
(17) Karolin, J.; Johansson, L. B.-A.; Strandberg, L.; Ny, T. *J. Am. Chem. Soc.* **1994**, *116*, 7801–7806.
(18) Tarahovsky, Y. S.; Koynova, R.; MacDonald, R. C. *Biophys. J.* **2004**, *87*, 1054–1064.
(19) Epand, R.; Vuong, P.; Yip, C. M.; Maekawa, S.; Epand, R. F. *Biochem. J.* **2004**, *379*, 527–532.
(20) Malinin, V. S.; Haque, Md. E.; Lentz, B. R. *Biochemistry* **2001**, *40*, 8292–8299.

Published on Web 08/05/2009

Scheme 1

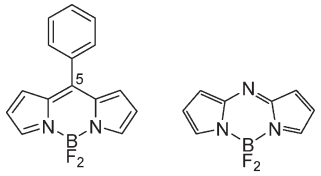

BODIPY dyes serve as energy-transfer donors to porphyrins[21−23] and other acceptors[24−28] in light-harvesting arrays. Ultrafast electron-transfer studies across supramolecular assemblies have appeared where BODIPY moieties act as electron donors[29] and acceptors.[30,31] BODIPY moieties having pendant Lewis bases, including amines, thioethers, and thiacrowns, are fluorescence metal-ion and NO sensors.[32−41] A recent account[42] describes triplet-state photosensitization with a di-iodo boron dipyrromethene, brought about by the heavy-atom effect of iodine, which enhances excited-state intersystem crossing.

Boron azadipyrromethenes (Scheme 1b) are fast regaining attention for their photophysical properties. Their signature optical features are absorptions centered near 300 and 620 nm with molar absorptivities in the tens of thousands. The longer-wavelength absorption falls just within an energy range suitable for human photodynamic therapy. Both transitions have interest for solar-energy capture. BF_2^+ chelates of azadipyrromethenes are fluorescent, and emission quantum yields can exceed 40%.[43] Introducing bromine atoms along the azadipyrromethene periphery begets triplet-state photochemistry. Photosensitization of O_2 occurs, and in vitro photokilling of human cervical carcinoma (HeLa) cells was reported.[44,45] These reports, combined with the red-absorption of boron azadipyrromethenes, suggest azadipyrromethenes as potent mediators of photodynamic therapy for cancers and other afflictions.

In the synthesis of boron dipyrromethenes and azadipyrromethenes, the conjugated skeleton is prepared first, and boron is added last. Clear opportunities exist for metal-ion binding, where the chromophore acts as a bidentate chelate. Metallocomplexes of dipyrromethenes have been investigated at some length; an emphasis has been supramolecular chemistry. Cohen and co-workers report six-coordinate tris(dipyrromethene) complexes of first-row transition elements[46−52] and group 13 ions.[53] In many such compounds a backbone *meso*-phenyl group bears Lewis basic sites. Porous coordination polymers form upon reaction with soluble metal-ion sources. Ultraviolet excitation of tris(5-mesityldipyrromethene) complexes of gallium and indium elicits green fluorescence with ns-scale lifetimes. Dolphin and collaborators[54,55] have published accounts of α- and *β*-linked dipyrromethenes in the construction of metallohelices and cyclic trimers of metal complexes. Bis(dipyrromethene)zinc(II) species have luminescence properties that are sensitive to rotational freedom of the *meso* substituent.[56] For example, bis(5-mesityldipyrromethene)zinc(II) emits with a fluorescence quantum yield $\Phi_{em} = 0.36$ at room temperature in toluene, whereas the 5-phenyl analogue is minimally fluorescent, $\Phi_{em} = 0.006$.[57] Bis(dipyrromethene)zinc complexes act as energy-transfer donors to zinc porphyrins in light-harvesting arrays.[58] Maeda and co-workers[59] have disclosed the nanoscale morphologies of (dipyrrinato)zinc complexes bearing *meso*-phenylene ethynylene moieties; some are luminescent.

More recently, reports of metal complexes of azadipyrromethenes have emerged. We have described homoleptic,

(21) Wagner, R. W.; Lindsey, J. S. *Pure Appl. Chem.* **1996**, *68*, 1373–1380.
(22) Wagner, R. W.; Lindsey, J. S.; Seth, J.; Palaniappan, V.; Bocian, D. F. *J. Am. Chem. Soc.* **1996**, *118*, 3996–3997.
(23) Li, F.; Yang, S. I.; Ciringh, Y.; Seth, J.; Martin, C. H.; Singh, D. L.; Kim, D.; Birge, R. R.; Bocian, D. F.; Holten, D.; Lindsey, J. S. *J. Am. Chem. Soc.* **1998**, *120*, 10001–10017.
(24) Yilmaz, M. D.; Bozdemir, O. A.; Akkaya, E. U. *Org. Lett.* **2006**, *8*, 2871–2873.
(25) Hepp, A.; Ulrich, G.; Schmechel, R.; von Seggern, H.; Ziessel, R. *Synth. Met.* **2004**, *146*, 11–15.
(26) Herrmann, A.; Weil, T.; Sinigersky, V.; Wiesler, U.-M.; Vosch, T.; Hofkens, J.; De Schryver, F. C.; Mullen, K. *Chem.—Eur. J.* **2001**, *7*, 4844–4853.
(27) Serin, J. M.; Brousmiche, D. W.; Fréchet, J. M. J. *Chem. Commun.* **2002**, 2605–2607.
(28) Serin, J. M.; Brousmiche, D. W.; Fréchet, J. M. J. *J. Am. Chem. Soc.* **2002**, *124*, 11848–11849.
(29) Harriman, A.; Rostron, J. P.; Cesario, M.; Ulrich, G.; Ziessel, R. *J. Phys. Chem. A* **2006**, *110*, 7994–8002.
(30) Hattori, S.; Ohkubo, K.; Urano, Y.; Sunahara, H.; Nagano, T.; Wada, Y.; Tkachenko, N. V.; Lemmetyinen, H.; Fukuzumi, S. *J. Phys. Chem. B* **2005**, *109*, 15368–15375.
(31) Kollmannsberger, M.; Rurack, K.; Resch-Genger, U.; Daub, J. *J. Phys. Chem. A* **1998**, *102*, 10211–10220.
(32) Zeng, L.; Miller, E. W.; Pralle, A.; Isacoff, E. Y.; Chang, C. J. *J. Am. Chem. Soc.* **2006**, *128*, 10–11.
(33) Ueno, T.; Urano, Y.; Kojima, H.; Nagano, T. *J. Am. Chem. Soc.* **2006**, *128*, 10640–10641.
(34) Gabe, Y.; Ueno, T.; Urano, Y.; Kojima, H.; Nagano, T. *Anal. Bioanal. Chem.* **2006**, *386*, 621–626.
(35) Gabe, Y.; Urano, Y.; Kikuchi, K.; Kojima, H.; Nagano, T. *J. Am. Chem. Soc.* **2004**, *126*, 3357–3367.
(36) Coskun, A.; Akkaya, E. U. *J. Am. Chem. Soc.* **2005**, *127*, 10464–10465.
(37) Turfan, B.; Akkaya, E. U. *Org. Lett.* **2002**, *4*, 2857–2859.
(38) Ulrich, G.; Ziessel, R. *J. Org. Chem.* **2004**, *69*, 2070–2083.
(39) Domaille, D. W.; Que, E. L.; Chang, C. J. *Nat. Chem. Biol.* **2008**, *4*, 168–175.
(40) Rurack, K.; Kollmannsberger, M.; Resch-Genger, U.; Daub, J. *J. Am. Chem. Soc.* **2000**, *122*, 968–969.
(41) Baruah, M.; Qin, W.; Vallée, R. A. L.; Beljonne, D.; Rohand, T.; Dehaen, W.; Boens, N. *Org. Lett.* **2005**, *7*, 4377–4380.
(42) Yogo, T.; Urano, Y.; Ishitsuka, Y.; Maniwa, F.; Nagano, T. *J. Am. Chem. Soc.* **2005**, *127*, 12162–12163.
(43) Loudet, A.; Bandichhor, R.; Wu, L.; Burgess, K. *Tetrahedron* **2008**, *64*, 3642–3654.
(44) Killoran, J.; Allen, L.; Gallagher, J. F.; Gallagher, W. M.; O'Shea, D. F. *Chem. Commun.* **2002**, 1862–1863.
(45) Gorman, A.; Killoran, J.; O'Shea, C.; Kenna, T.; Gallagher, W. M.; O'Shea, D. F. *J. Am. Chem. Soc.* **2004**, *126*, 10619–10631.
(46) Halper, S. R.; Do, L.; Stork, J. R.; Cohen, S. M. *J. Am. Chem. Soc.* **2006**, *128*, 15255–15268.
(47) Halper, S. R.; Cohen, S. M. *Inorg. Chem.* **2005**, *44*, 486–488.
(48) Murphy, D. L.; Malachowski, M. R.; Campana, C. F.; Cohen, S. M. *Chem. Commun.* **2005**, 5506–5508.
(49) Halper, S. R.; Cohen, S. M. *Inorg. Chem.* **2005**, *44*, 4139–4141.
(50) Halper, S. R.; Malachowski, M. R.; Delaney, H. M.; Cohen, S. M. *Inorg. Chem.* **2004**, *43*, 1242–1249.
(51) Halper, S. R.; Cohen, S. M. *Chem.—Eur. J.* **2003**, *9*, 4661–4669.
(52) Cohen, S. M.; Halper, S. R. *Inorg. Chim. Acta* **2002**, *341*, 12–16.
(53) Thoi, V. S.; Stork, J. R.; Magde, D.; Cohen, S. M. *Inorg. Chem.* **2006**, *45*, 10688–10697.
(54) Zhang, Y.; Thompson, A.; Rettig, S. J.; Dolphin, D. *J. Am. Chem. Soc.* **1998**, *120*, 13537–13538.
(55) Thompson, A.; Rettig, S. J.; Dolphin, D. *Chem. Commun.* **1999**, 631–632.
(56) Sutton, J. M.; Rogerson, E.; Wilson, C. J.; Sparke, A. E.; Archibald, S. J.; Boyle, R. W. *Chem. Commun.* **2004**, 1328–1329.
(57) Sazanovich, I. V.; Kirmaier, C.; Hindin, E.; Yu, L.; Bocian, D. F.; Lindsey, J. S.; Holten, D. *J. Am. Chem. Soc.* **2004**, *126*, 2664–2665.
(58) Yu, L.; Muthukumaran, K.; Sazanovich, I. V.; Kirmaier, C.; Hindin, E.; Diers, J. R.; Boyle, P. D.; Bocian, D. F.; Holten, D.; Lindsey, J. S. *Inorg. Chem.* **2003**, *42*, 6629–6647.
(59) Maeda, H.; Hasegawa, M.; Hashimoto, T.; Kakimoto, T.; Nishio, S.; Nakanisi, T. *J. Am. Chem. Soc.* **2006**, *128*, 10024–10025.

bis-chelate complexes of Zn^{II} and Hg^{II}.[60] The zinc complexes share several structural commonalities with dipyrromethene complexes, though the dihedral angle of the two chelate rings is strongly influenced by intramolecular $\pi-\pi$ interactions between a pyrrole and a substituent phenyl ring. The four-coordinate group 12 complexes display more intense visible absorption maxima that are red-shifted relative to the free ligands; the complexes are non-emissive at room temperature. Complexes of the tetraphenylazadipyrromethene with first-row ions Co^{II}, Ni^{II}, and Cu^{II}, along with the Zn^{II} complex we reported, appeared later.[61] As with Zn^{II}, complexation of these other divalent first-row metals results in pronounced changes in the absorption spectra.

A second class of azadipyrromethene coordination compounds are the three-coordinate, group 11 complexes disclosed earlier.[62] These contain a d^{10} M^{I} (M = Cu, Ag, Au) center chelated by tetraphenylazadipyrromethene, with triphenylphosphine (PPh_3) bound to the third coordination site, resulting in an essentially trigonal planar geometry. The low-energy absorption maximum intensifies and red-shifts in the group 11 complexes relative to the parent ligand. All three are weakly emissive at room temperature, displaying emission maxima of ~650 nm and < 1% quantum yields. Preliminary density functional theory (DFT) calculations on the silver complex indicate primarily ligand-centered frontier orbitals and electronic transitions.

Here, we detail the synthesis, characterization, and photophysical properties of an extended series of group 11 azadipyrromethene complexes. All but one are structurally characterized by single crystal X-ray diffraction, whereas spectral methods and microanalysis verify the purity of all products. Included are Cu^{I} and Ag^{I} complexes with methoxy-substituted azadipyrromethenes; substitution of the pendant aryl rings perturbs the complexes' absorption spectra. We also describe Ag^{I} derivatives where triethylphosphine replaces triphenylphosphine as the capping ligand. We enumerate the structural and spectral consequences of inserting this smaller phosphine, which cannot participate in the intramolecular $\pi-\pi$ interactions that are common in PPh_3-bound complexes. Room temperature absorption and emission spectra are reported for all compounds. The trends in the absorption and emission spectra noted earlier,[60] namely, the intensified and red-shifted maxima relative to free ligand, recur in the derivatives described here. DFT and time-dependent DFT calculations find the visible absorptions of azadipyrromethene complexes to be ligand-centered; metal-ion involvement is peripheral.

Results and Discussion

Syntheses. Scheme 2 details the synthesis of the azadipyrromethene complexes considered here; Table 1 collects optimized yields. Reaction conditions were analogous to those previously employed in the syntheses of PPh_3CuL_a (**1**) and PPh_3AgL_a (**4**).[62] Complexes of copper(I) and silver(I) assembled rapidly in room-temperature reactions of (phosphine)metal(I) triflates with the free

Scheme 2

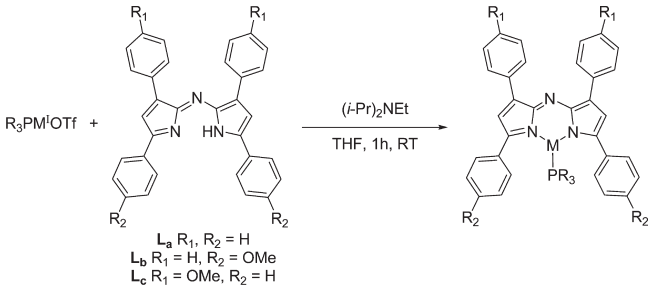

azadipyrromethene in the presence of diisopropylethylamine. (Triphenylphosphine)copper(I) triflate was generated *in situ* from free triphenylphosphine and the toluene adduct of copper(I) triflate. Likewise, (triethylphosphine)silver(I) triflate was prepared *in situ* from silver triflate and a slight excess of triethylphosphine. As described previously,[62] Au^{I} complex **9** is prepared by *in situ* deprotonation of tetraphenylazadipyrromethene, followed by metathesis with $Au^{I}(PPh_3)Cl$. Tetrahydrofuran (THF) solutions of the free azadipyrromethene are dark blue; upon metalation, the color changes to a somewhat brighter blue. Syntheses of Cu^{I} and Ag^{I} complexes are complete in 60 min, as judged by NMR, and isolated yields range from 62−89%. All complexes have been characterized by ^{1}H and ^{31}P NMR spectroscopy, absorption and emission spectroscopy, and elemental analysis; crystal structures of eight have been determined.

Azadipyrromethene ^{1}H NMR spectra are largely insensitive to copper(I) or silver(I) binding.[62] The lone exceptions are the resonances associated with the azadipyrromethene phenyl rings closest to the metal−phosphine fragment in triphenylphosphine complexes. These resonances shift upfield by 0.3−0.7 ppm upon complexation, and the methoxy singlet in bound L_b also shifts upfield by a similar amount for **2** and **5**. Resonances of triphenylphosphine ligands in **1**−**6** and **9** are essentially invariant; they overlap with azadipyrromethene resonances. The $^{31}P\{^{1}H\}$ NMR spectra show significantly broadened resonances, and in the silver complexes the expected doublet of doublets splitting pattern, arising from ^{31}P coupling to ^{107}Ag and ^{109}Ag (51.8% and 48.2% abundant, respectively), is unresolved.

Crystal Structures. Structures of **1**−**5** and **7**−**9** have been determined crystallographically. Those of **1**, **4**, and **9** were reported previously.[62] No complex possesses crystallographically imposed symmetry. All structures contain discrete molecules with three-coordinate metal centers. Coordination geometries are approximately trigonal planar, though in all cases the N—M—N bond angles are decidedly smaller than the N—M—P angles. Thermal ellipsoid projections for PPh_3CuL_b (**2**), PPh_3AgL_b (**5**), and PEt_3AgL_c (**8**) appear in Figure 1. Table 2 summarizes crystallographic data for the new azadipyrromethene complexes reported here.

Table 3 collects selected average interatomic distances and angles for the complexes of Cu^{I}(**1**−**3**) and Ag^{I}(**4**, **5**, **7**, and **8**), as well as the corresponding distances for Au^{I} complex **9**. Metal−nitrogen bond distances range from 1.9784(13)−1.9914(14) Å (M = Cu^{I}), 2.2073(12)−2.2811(19) Å (M = Ag), and 2.2349(12) and 2.2448(12) Å (M = Au, **9**). In all compounds, slight asymmetries in

(60) Teets, T. S.; Partyka, D. V.; Updegraff, J. B., III; Gray, T. G. *Inorg. Chem.* **2008**, *47*, 2338–2346.
(61) Palma, A.; Gallagher, J. F.; Müller-Bunz, H.; Wolowska, J.; McInnes, E. J. L.; O'Shea, D. F. *Dalton Trans.* **2009**, 273–279.
(62) Teets, T. S.; Partyka, D. V.; Esswein, A. J.; Updegraff, J. B., III; Zeller, M.; Hunter, A. D.; Gray, T. G. *Inorg. Chem.* **2007**, *46*, 6218–6220.

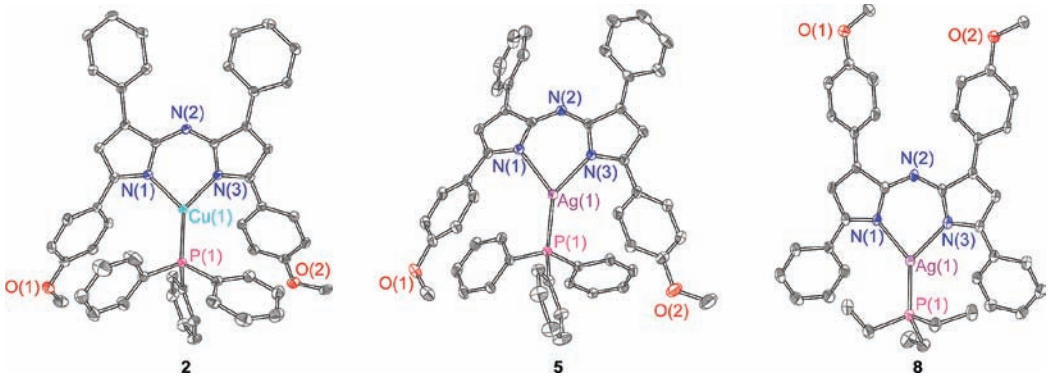

Figure 1. X-ray crystal structures of **2**, **5**, and **8**. Thermal ellipsoids appear at the 50% probability level; data were collected at 100 K. Hydrogen atoms are omitted for clarity, and carbon atoms, shown in gray, are unlabeled.

Table 1. Syntheses and Designation of Compounds

Product no.	Metal(I) precursor	Ligand	Product	Isolated yield
1	$Ph_3PCuOTf$	L_a	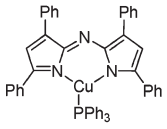	89%
2	$Ph_3PCuOTf$	L_b	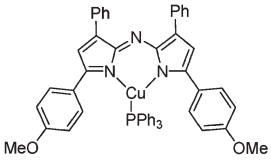	76%
3	$Ph_3PCuOTf$	L_c	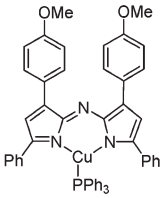	79%
4	$Ph_3PAgOTf$	L_a	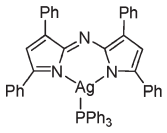	62%
5	$Ph_3PAgOTf$	L_b	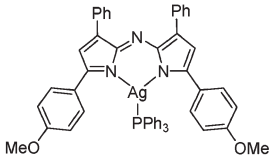	67%
6	$Ph_3PAgOTf$	L_c	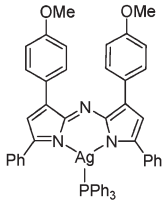	68%
7	$Et_3PAgOTf$	L_a	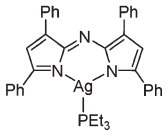	65%
8	$Et_3PAgOTf$	L_c	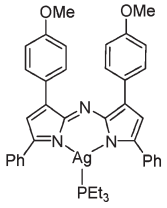	69%

M−N bond lengths occur. The most asymmetric (azadipyrromethene)M^I grouping, in terms of bond lengths to nitrogen, is one crystallographically independent molecule of **5**, where the discrepancy in Ag−N bond lengths is 0.07 Å. Compound **3** has the most nearly equal M−N bond lengths with the difference being 0.003 Å. Metal−phosphorus bond lengths in homologous compounds are 2.1800(5) Å (**1**), 2.3503(6) Å (**4**, averaged over three independent molecules), and 2.2088(3) Å (**9**). Corresponding bond lengths to phosphorus in other compounds are similar; substitution of PPh_3 in **4** with PEt_3 in **7** does not significantly alter the Ag−P bond length. Methoxy-substitution on the azadipyrromethene elicits small and non-systematic changes in metal−ligand bond lengths and angles. Structural comparisons with related compounds suggest that the bond metrics encountered here are not unusual. For example, copper(I)−nitrogen bond lengths in bis(2,9-diphenyl-3,4,7,8-tetramethyl-1,10-phenanthroline)copper(I) tetraphenylborate range from 1.993(3)−2.150(3) Å[63] and those in a bis(2,9-pentafluorophenyl-1,10-phenanthroline)copper(I) cation fall between 2.048(3) and 2.109(3) Å.[64] In mixed phenanthroline-chelating diphosphine copper(I) complexes, Cu−N bond lengths range from 2.064(3)−2.109(2) Å.[65] Structures of two three-coordinate (bipyridine)silver(I) phosphine cations are available. Silver−nitrogen bond lengths

(63) Cunningham, C. T.; Moore, J. T.; Cunningham, K. L. H.; Fanwick, P. E.; McMillin, D. R. *Inorg. Chem.* **2000**, *39*, 3638–3644.
(64) Hamilton, C. W.; Laitar, D. S.; Sadighi, J. P. *Chem. Commun.* **2004**, 1628–1629.
(65) Kuang, S.-M.; Cuttell, D. G.; McMillin, D. R.; Fanwick, P. E.; Walton, R. A. *Inorg. Chem.* **2002**, *41*, 3313–3322.

Table 2. Crystallographic Data for Phosphine-ligated Azadipyrromethene Complexes

	2	**3**	**5**	**7**	**8**
Formula	$C_{52}H_{41}CuN_3O_2P$	$C_{52}H_{41}CuN_3O_2P$	$C_{52}H_{41}AgN_3O_2P$	$C_{38}H_{37}AgN_3P$	$C_{40}H_{41}AgN_3O_2P$
fw	834.42	834.42	877.2	674.56	734.61
crystal system	triclinic	monoclinic	triclinic	triclinic	triclinic
space group	$P\bar{1}$	$P2_1/n$	$P\bar{1}$	$P\bar{1}$	$P\bar{1}$
a, Å	15.0069(3)	12.1711(8)	13.8159(5)	11.3616(3)	11.4051(8)
b, Å	17.9641(4)	14.1525(9)	17.4106(6)	11.4783(3)	11.7105(9)
c, Å	19.0956(4)	23.9305(16)	19.3928(7)	13.0739(3)	15.7693(12)
α, deg	82.9370(10)		75.636(2)	88.607(1)	110.336(3)
β, deg	73.2040(10)	92.4870(10)	88.549(2)	73.817(1)	102.065(3)
γ, deg	67.2250(10)		85.457(2)	73.256(1)	89.987(4)
cell volume, Å^3	4543.68(17)	4118.2(5)	4504.7(32)	1565.10(7)	1925.2(2)
Z	4	4	4	2	2
D_{calcd}, Mg m^{-3}	1.334	1.346	1.296	1.415	1.267
T, K	100(2)	100(2)	100(2)	100(2)	100(2)
μ, mm^{-1}	0.564	0.616	0.525	0.726	0.600
F(000)	1904	1736	1808	675	760
cryst size, mm^3	0.36 × 0.26 × 0.20	0.33 × 0.19 × 0.18	0.50 × 0.30 × 0.13	0.17 × 0.14 × 0.13	0.48 × 0.30 × 0.25
θ_{min}, θ_{max}, deg	1.23, 28.39	1.67, 27.50	1.48, 34.02	1.95, 33.21	1.83, 27.50
no. of reflns collected	22509	47402	131614	32210	30783
no. of indep reflns	18999	9426	36074	11642	8775
no. of refined params	1175	534	1067	420	429
goodness-of-fit on F^{2a}	1.030	1.027	1.079	1.102	1.064
final R indices^b [$I > 2\sigma(I)$] R_1	0.0355	0.0300	0.0373	0.0382	0.0570
wR_2	0.0948	0.0738	0.1120	0.1114	0.1491
R indices (all data)					
R_1	0.0445	0.0386	0.0482	0.0470	0.0597
wR_2	0.1014	0.0782	0.1053	0.1005	0.1528

[a] GOF = $[\sum w(F_o^2 - F_c^2)^2/(n-p)]^{1/2}$; n = number of reflections, p = number of parameters refined. [b] $R_1 = \sum(||F_o| - |F_c||)/\sum|F_o|$; $wR_2 = [\sum w(F_o^2 - F_c^2)^2/\sum wF_o^4]^{1/2}$.

Table 3. Selected Interatomic Distances (Å) and Angles (deg) for Group 11 Azadipyrromethene Complexes **1**−**9**

	Cu^{Ia}	Ag^{Ib}	Au^{Ic}
d(M−N)	1.9854(13)	2.2423(17)	2.2398(12)
d(M−P)	2.1776(4)	2.3403(9)	2.2088(3)
∠(N−M−N)	94.06(5)	83.11(6)	81.51(4)

[a] Average for **1**−**3**. [b] Average for **4**, **5**, **7**, and **8**. [c] Complex **9**; M−N bonds are averaged.

in two salts of $[Ag(bpy)(PPh_3)]^+$ range from 2.251(3)−2.316(4) Å.[66] In a dinuclear complex[67] where 1,4-bis(diphenylphosphino)butane bridges two Ag(bpy)^I cations, Ag−N bond lengths are 2.227(3) and 2.334(3) Å.

Metal-ion binding dilates the backside C−N$_{meso}$−C linkage away from the ideal 120° for sp^2-hybridization. For example, these angles about the *meso*-nitrogen in $\mathbf{L_c}$ complexes **3** and **8** are 127.60(13)° and 128.3(2)°, respectively. For comparison, O'Shea and co-workers report a C−N$_{meso}$−C angle of 119.7(3)° for the corresponding BF_2^+-chelate of $\mathbf{L_c}$. These ligand distortions suggest strain in group 11 azadipyrromethene complexes, but also that the ligand is pliant enough to accommodate large cations such as Ag^I (which is bigger than Au^I).[68]

The metal-ion coordination geometry in **1**−**5** and **7**−**9** is trigonal planar. The coordination plane tilts relative to the best-fit plane of the central azadipyrromethene skeleton. This tilting can be described as the angle between the mean plane of the azadipyrromethene core (the two pyrroles and bridging nitrogen) and the plane defined by the N−M−N chelate. Figure 2 depicts this canting for silver(I) complex **8**, where the interplanar angle is 27.0°. The largest such tilt encountered here is 29.8° for gold complex **9**; the smallest is 18.3° for one crystallographically independent molecule of **4**. Substitution of PPh_3 (cone angle = 145°),[69] with less bulky PEt_3 (cone angle = 132°) does not decrease the tilt of the coordination plane, as judged from a comparison of the structures of **4** and **7**. At least for this one example, ligand tilting likely results from a size mismatch between the M^I ion and the binding cavity. Furthermore, we note that these angles vary considerably across the series, even for complexes with the same metal ion. The structures of **2**, **4**, and **5** contain two, three, and two molecules per asymmetric unit, respectively. In these instances, crystallographically independent molecules of the same complex possess disparate tilting angles, differing by more than 2.7°. These observations indicate that the structure is quite flexible, and that the crystallographically observed canting angle is not rigidly imposed.

Ligand bite angles, defined as the N−M−N angle for bound azadipyrromethenes, are 94.49(6)° for **1**, 86.24(7), 82.96(7), and 82.27(7) for the three crystallographically independent molecules of **4**, and 81.54(4)° for **9**. The range for all compounds is 81.51(4)° for **9** to 95.12(5) for **3**, and a decrease is observed traversing down the group 11 series from copper(I) to silver(I) to gold(I). For comparison, the bite angle in bis(2,9-diphenyl-3,4,7,8-tetramethyl-1,10-phenanthroline)copper(I) tetraphenylborate is 81.23(11)°,[63] and this angle is representative of those in other cuprous phenanthroline complexes.[64,65,70] In the

(66) Khalaji, A. D.; Amirnasr, M.; Aoki, K. *Anal. Sci.* **2006**, *22*, x87–x88.
(67) Zhang, L.; Chen, C.; Zhang, Q.; Zhang, H.; Kang, B. *Acta Crystallogr.* **2003**, *E59*, m536–m537.
(68) Bayler, A.; Schier, A.; Bowmaker, G. A.; Schmidbaur, H. *J. Am. Chem. Soc.* **1996**, *118*, 7006–7007.
(69) Tolman, C. A. *Chem. Rev.* **1977**, *77*, 313–348.
(70) Miller, M. T.; Gantzel, P. K.; Karpishin, T. B. *Inorg. Chem.* **1998**, *37*, 2285–2290.

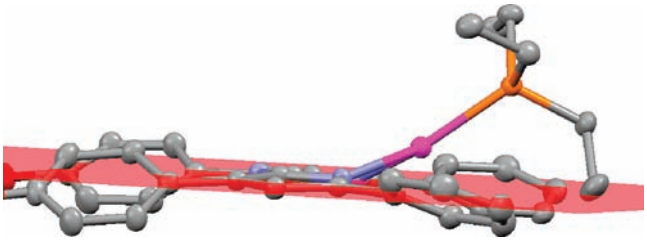

Figure 2. View of the crystal structure of **8** showing the canting of the N−Ag−N plane relative to the mean plane of the ligand. The plane depicted in red indicates the mean plane of the azadipyorromethene ligand (the two pyrrole rings and the bridging nitrogen).

three-coordinate silver(I) complex $[Ag(bpy)(PPh_3)]^{2+}$, the N−Ag−N bite angle is 73.0(1)° for both the perchlorate and hexafluorophosphate salts.[66] In the disilver variant $[Ag_2(bpy)_2\mu_2\text{-}(dppb)](BF_4)_2$, the corresponding bite angle is 72.08(10)°.[67] At parity of metal ion, the trend is toward larger bite angles in azadipyrromethene ligands than for either bipyridyl or phenanthroline in analogous complexes. Metal−nitrogen bond lengths (vide supra) are similar for diimine and azadipyrromethene ligands.

Inter- and intramolecular π-stacking is prominent in metalla-azadipyrromethene crystal structures. Among triphenylphosphine complexes, π-stacking of a phosphorus phenyl substituent and one proximal benzene ring of the azadipyrromethene recurs. For example, the centroid of one 4-methoxyphenyl group in an independent molecule of **2** approaches the best-fit plane of a phosphine phenyl group (in the same molecule) within 3.53 Å. Similar stacking occurs in other structures. In the crystal structure of **1**, two distal phenyl groups in molecules related by an inversion center approach with centroids separated by 3.71 Å. Our earlier communication notes a similar bimolecular stacking in symmetry-related molecules of **9** where ring-centroids are separated by 3.69 Å.[62] Such interactions appear in other structures, and there is no apparent correlation with ring-substitution of the azadipyrromethene. NMR evidence is consistent with persistence of the intramolecular π-stacking interactions in solution.[71] Resonances associated with the "proximal" azadipyrromethene phenyl rings, which undergo π-stacking with PPh_3 in the solid state, show a pronounced 0.3−0.7 ppm upfield shift at room temperature in $CDCl_3$ solution, whereas the same resonances in the PEt_3-bound complexes only shift by ~0.1 ppm.

Optical Properties. Recent investigations of boron azadipyrromethenes have emphasized light absorption and emission. A persistent context has been photodynamic therapy. Clinical utility of boron azadipyrromethenes or other triplet-state photosensitizers requires absorptivity between about 600−900 nm. Light of these wavelengths effectively penetrates human flesh; the longer wavelength limit is fixed by the excitation energy of promoting $^3O_2$ to its singlet excited state for therapeutic action. Boron azadipyrromethenes absorb strongly between 650−700 nm with molar extinction coefficients in $CHCl_3$ of 75 000 M^{-1} cm^{-1} or greater. A corresponding emission profile mirrors this absorption. Typical Stokes shifts are 20−40 nm red of the absorption maximum.[45]

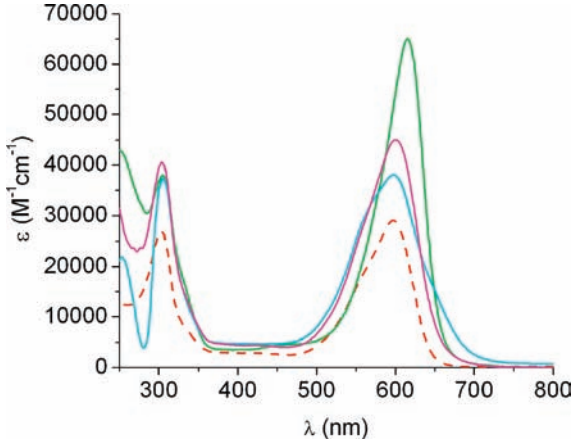

Figure 3. Room-temperature absorption spectra of $\mathbf{L_a}$ (red, dashed line), **1** (light blue), **4** (green), and **9** (magenta), recorded in $CHCl_3$.

Table 4. Summary of Absorption Wavelengths (nm) and Molar Absorptivities (M^{-1} cm^{-1}) for all Azadipyrromethene Ligands and Complexes[a]

	λ_{max}, ε (near-UV)	λ_{max}, ε (red)
$\mathbf{L_a}$	303, 27 000	597, 29 000
$\mathbf{L_b}$	278, 68 000	619, 37 000
$\mathbf{L_c}$	291, 36 000	608, 36 000
1	305, 38 000	597, 38 000
2	320, 24 000	620, 28 000
3	306, 32 000	606, 38 000
4	306, 30 000	615, 65 000
5	324, 30 000	631, 69 000
6	304, 39 000	615, 64 000
7	304, 30 000	610, 42 000
8	303, 31 000	614, 46 000
9	304, 40 000	600, 45 000

[a] Measured in $CHCl_3$ at room temperature.

Group 11 metal-ion complexes of azadipyrromethene ligands substantially retain the optical properties of their boron analogues. Figure 3 depicts absorption spectra of homologous complexes **1**, **4**, and **9**, together with free $\mathbf{L_a}$; Table 4 summarizes absorption maxima of all compounds. A near-UV feature is present in all of the ligands and complexes; this feature red-shifts for ligands bearing a methoxy substituent on the proximal phenyl ring (complexes **2** and **5**, Table 4). This reddening of the higher-energy absorption also takes place in zinc bis(azadipyrromethenes). It originates from proximal phenyl-group participation in the ligand-centered transitions that elicit this near-UV feature.[60] An intense visible absorption in the red region of the spectrum ($\varepsilon \sim 30\,000$ M^{-1} cm^{-1}) is characteristic of azadipyrromethene ligands; a shoulder is evident near 550 nm. Upon complexation this absorption intensifies markedly; for silver complex **4**, the extinction coefficient at λ_{max} more than doubles ($\varepsilon = 65\,000$ M^{-1} cm^{-1}). The amplification of the molar absorptivity is not as dramatic for Cu^I and Au^I complexes, and is also less pronounced for PEt_3Ag^I complexes **7** and **8**. For Cu^I complexes **1**−**3**, the position of the visible absorption maximum is nearly identical to that of the free azadipyrromethene. For Ag^I complexes **4**−**8** , the visible absorption maximum bathochromically shifts; the largest such shift is 18 nm in **4** relative to $\mathbf{L_a}$. For Au^I complex **9**, the visible absorption maximum red-shifts by 3 nm from that of tetraphenylazadipyrromethene. Methoxy-substituted

(71) Martin, C. B.; Mulla, H. R.; Willis, P. G.; Cammers-Goodwin, A. *J. Org. Chem.* **1999**, *64*, 7802–7806.

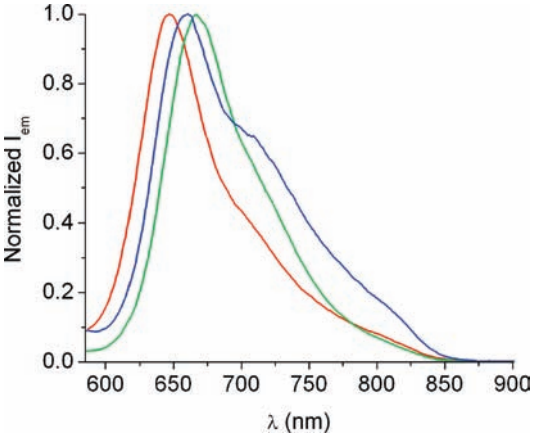

Figure 4. Normalized room temperature emission spectra for **4** (red), **5** (green), and **6** (blue), recorded at room temperature in deoxygenated $CHCl_3$ solution at micromolar concentrations with 550 nm excitation.

ligands and complexes typically show red-shifted visible absorption maxima compared to their unsubstituted analogues; this perturbation in the absorption spectrum is considerably more pronounced when the methoxy group is positioned on the proximal phenyl ring (i.e., the phenyl substituent derived from acetophenone), as in $\mathbf{L_b}$ and complexes **2** and **5**. The intensity of the visible absorption bands is not affected by the presence or absence of methoxy groups on the pendant phenyl rings. As described earlier,[62] at 77 K in 2-methyltetrahydrofuran glass the absorption features are much better resolved, and at least three distinct maxima in the red region of the spectrum are evident for complexes **1**, **4**, and **9**.

Absorption spectra of the new complexes bear similarities to those of our earlier zinc(II) and mercury(II) bis(azadipyrromethenes)[60] and to the M(II) complexes of O'Shea and collaborators.[61] In bis(azadipyrromethene) complexes, visible absorption maxima approximately coincide with that of the free ligand, and with maxima of the new complexes reported here. Molar absorptivities at λ_{max} are roughly twice those of the free ligand. Group 11 mono(azadipyrromethenes) show a single asymmetric visible absorption band, whereas bis(azadipyrromethene) complexes of 3d-metals (but not mercury) show a partial splitting that is clearly resolved for $Cu^{II}(\mathbf{L_a})_2$. The near-ultraviolet absorption maximum is similar across boron complexes and mono- and bis(azadipyrromethene) complexes. Substituent effects on these higher-energy transitions were discussed earlier.[60]

Azadipyrromethene complexes of the d^{10} metal ions of group 11 are luminescent. Room-temperature excitation in chloroform elicits weak emission that mirrors the absorption profile near 600 nm, with average Stokes shifts of 41 nm for **1**−**9**. The small Stokes shift suggests a fluorescence origin of the emission. Excitation spectra parallel absorption spectra. Figure 4 depicts normalized room temperature emission spectra of Ag^I complexes **4**−**6,** which are representative of the complexes described here. Absorption and emission spectra for complexes **1** − **9** are deposited as Supporting Information (Figures S1−S9); optical spectra of **1**, **4**, and **9** were previously communicated.[62] As shown in Figure 4, methoxy substitution leads to a red-shift in the emission maximum, and again substitution at the proximal phenyl ring has the greater effect. Also, the distinct shoulder that is evident in the spectrum of **6** appears in the spectra of azadipyrromethene ligand $\mathbf{L_c}$ and its other complexes **3** and **8**. The room temperature emission spectra of the complexes are similar to those of the free ligands, and are not severely altered by changing the metal. In addition, replacing PPh_3 in **4** and **6** with PEt_3 in **7** and **8** does not modulate the luminescence features. Emission quantum yields are also very similar to those of the free azadipyrromethenes. $PPh_3Ag\mathbf{L_b}$ (**5**), $\Phi_{em} = 0.012$, was the only metal complex with a quantum yield exceeding 1%. Table 5 summarizes the emission wavelengths and quantum yields for all ligands and complexes at room temperature. As discussed previously,[62] emission spectra of **1**, **4**, and **9** measured at 77 K in 2-methyltetrahydrofuran glass display structured luminescence, with average peak-to-peak separations consistent with azadipyrromethene skeletal modes.[72] The inefficient emission found at room temperature may result from the rotational freedom of the four pendant benzene rings, and possibly from the ancillary phosphine ligands; conformationally restrained azadipyrromethenes fluoresce with higher yields.[73,74]

Table 5. Summary of Emission Maxima and Quantum Yields for All Complexes[a]

	λ_{em} (nm)	Φ_{em}
$\mathbf{L_a}$	642	0.0014
$\mathbf{L_b}$	662	0.014
$\mathbf{L_c}$	660, 707 (sh)	0.0020
1	642	0.0025
2	665	0.0067
3	667, 705 (sh)	0.0024
4	647	0.0039
5	667	0.012
6	660, 705 (sh)	0.0034
7	645	0.0021
8	642	0.0030
9	645	0.0024

[a] Measured in optically dilute deoxygenated $CHCl_3$ solutions at room temperature with 550 nm excitation.

Calculations. DFT calculations have been performed on the neutral ligand $\mathbf{L_a}$ (where one pyrrole nitrogen is protonated) and on the model complexes $(H_3P)M^I\mathbf{L_a}$ (M = Cu, Ag, Au). Table S1 (Supporting Information) collects calculated interatomic distances alongside average values found crystallographically for **1**, **4**, and **9**. Root-mean square and average deviations are indicated. Save for gold complex **9**, optimized metrics compare favorably with crystallographic values. In **9**, microsymmetry about gold is essentially C_{2v} with a small difference (0.01 Å) in the Au−N bond lengths. The calculated structure predicts asymmetric gold ligation, with Au−N bond lengths that differ by 0.385 Å. Gold(I) in the optimized structure is pseudo-two coordinate with one P−Au−N angle calculated at 162.3°. The more distant pyrrole nitrogen perturbs the binding of gold from an idealized linearity, but the calculation fails to reproduce the observed trigonal coordination. Geometry optimization of a model complex where Ph_3PAu^+ coordinates a

(72) Li, X.-Y.; Czernuszewicz, R. S.; Kincaid, J. R.; Su, Y. O.; Spiro, T. G. *J. Phys. Chem.* **1990**, *94*, 31–47.
(73) Zhao, W.; Carreira, E. M. *Angew. Chem., Int. Ed.* **2005**, *44*, 1677–1679.
(74) Loudet, A.; Bandichhor, R.; Burgess, K.; Palma, A.; McDonnell, S. O.; Hall, M. J.; O'Shea, D. F. *Org. Lett.* **2008**, *10*, 4771–4774.

variant of $\mathbf{L_a}$ where hydrogen replaces the remote phenyl groups converges to a similar quasi-linear coordination geometry. The cause of three-coordination of gold in **9** remains unresolved. The possibility that crystal-packing interactions determine the solid-state structure cannot be excluded, though the solution ^{1}H NMR spectrum is consistent with a C_s-symmetric structure. Discussion henceforth will consider only **1** and **4**, along with free $\mathbf{L_a}$ and its BF_2^+ adduct.

Time-dependent DFT computations were performed using the statistical averaging of (model) orbital potentials (SAOP)[75−77] on geometries optimized with the revised Perdew−Becke−Ernzerhof functional.[78,79] Response calculations include implicit solvation through the conductor-like screening model of Klamt and coworkers.[80−82] Vertical excitation wavelengths, oscillator strengths, and orbital compositions of the excited states were calculated.

In boron azadipyrromethenes, the optical transitions of interest to photodynamic therapy center near 620 nm with extinction coefficients reaching past 70 000 M^{-1} cm^{-1}. Similar absorptions recur in metallocomplexes and in the free ligand with lesser intensity. Figure 5 depicts a partial Kohn−Sham orbital energy-level diagram of the model copper complex $PH_3Cu\mathbf{L_a}$; plots of selected orbitals appear as Figure 5(b). Time-dependent DFT calculations indicate that multiple electronic transitions combine to produce these absorptions. For all compounds, the lowest several allowed transitions are to the lowest-occupied Kohn−Sham orbital (LUMO), consistent with the large one-electron energy separation between it and the LUMO + 1. In the free ligand, the LUMO←HOMO and LUMO←HOMO − 1 transitions intermix through configuration interaction. Much the same arrangement prevails in BF_2^+ and group 11 chelates. For example, in the model copper(I) complex $PH_3Cu\mathbf{L_a}$ HOMO←LUMO and HOMO←LUMO − 3 transitions undergo configuration interaction and yield vertical excitations of high oscillator strength. The orbitals involved are entirely analogous to those of the free ligand with minimal participation of copper.

The visible absorption maxima of azadipyrromethene complexes red-shift with *para*-methoxy substitution of either the proximal or the distal phenyl substituents, cf., Table 4. This effect has been noted previously,[45] and is more pronounced for substitution at the proximal (to copper) phenyls. Time-dependent DFT calculations capture the red-shifting effect of methoxy substitution. The transitions with the highest oscillator strength move 18 nm to lower energy for $PH_3Cu\mathbf{L_b}$ relative to the complex of $\mathbf{L_a}$, and a lesser red-shift is calculated for $PH_3Cu\mathbf{L_c}$.

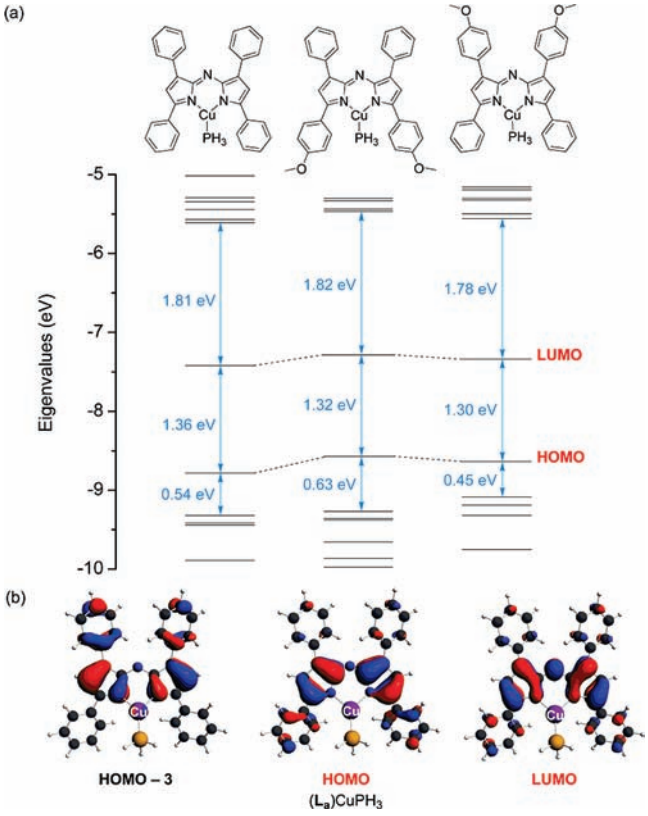

Figure 5. (a) Partial Kohn−Sham orbital eigenvalue diagram of model complexes $PH_3Cu\mathbf{L_{a-c}}$. Implicit chloroform solvation is included through a conductor-like screening model. (b) Plots of selected orbitals of $(H_3P)Cu\mathbf{L_a}$ (contour level 0.03 au).

The energy-level diagram of Figure 5 suggests an explanation. Methoxy substitution destabilizes the HOMO and LUMO of $\mathbf{L_b}$ and $\mathbf{L_c}$ complexes, compared to those of $\mathbf{L_a}$; the HOMO rises slightly more in energy than the LUMO.[83] Thus, *para*-methoxy substitution shrinks the HOMO−LUMO gap, in a manner consistent with the red-shifted absorptions found experimentally. The orbital plots of Figure 5(b) show amplitude on the *para* carbon atoms of the HOMO and LUMO of $PH_3Cu\mathbf{L_a}$, suggesting that both orbitals respond to substitution at these positions. The greater orbital amplitude rests at the *para* carbon of the proximal phenyl rings, and substitution here is more red-shifting than at the distal centers.

Azadipyrromethene electronic transitions are interpretable within a three-orbital model, Scheme 3. As in the spectra of porphyrin species,[84−86] the most prominent features result from transitions undergoing configuration interaction. In Scheme 3, state designations refer to the C_{2v}-symmetric boron complex **10**. Time-dependent calculation of **10** predicts a pair of intense absorptions, each having the same two constituent excitations. These are the

(75) Schipper, P. R. T.; Gritsenko, O. V.; van Gisbergen, S. J. A.; Baerends, E. J. *J. Chem. Phys.* **2000**, *112*, 1344–1352.
(76) Gritsenko, O. V.; Schipper, P. R. T.; Baerends, E. J. *Chem. Phys. Lett.* **1999**, *302*, 199–207.
(77) Grüning, M.; Gritsenko, O. V.; van Gisbergen, S. J. A.; Baerends, E. J. *J. Chem. Phys.* **2002**, *116*, 9591–9601.
(78) Perdew, J. P.; Burke, K.; Ernzerhof, M. *Phys. Rev. Lett.* **1996**, *77*, 3865–3868.
(79) Hammer, B.; Hansen, L. B.; Norskov, J. K. *Phys. Rev. B* **1999**, *59*, 7413–7421.
(80) Klamt, A.; Schüürmann, G. *J. Chem. Soc., Perkin Trans. 2* **1993**, 799–805.
(81) Klamt, A. *J. Phys. Chem.* **1995**, *99*, 2224–2235.
(82) Klamt, A.; Jones, V. *J. Chem. Phys.* **1996**, *105*, 9972–9981.
(83) Abbreviations: HOMO, highest occupied Kohn−Sham orbital; LUMO, lowest unoccupied Kohn−Sham orbital.
(84) Gouterman, M. Optical spectra and electronic structure of porphyrins and related rings. In *The Porphyrins*; Dolphin, D., Ed.; Academic Press: New York, 1978; pp 1−165
(85) Loh, Z.-H.; Miller, S. E.; Chang, C. J.; Carpenter, S. D.; Nocera, D. G. *J. Phys. Chem. A* **2002**, *106*, 11700–11708.
(86) Partyka, D. V.; Robilotto, T. J.; Zeller, M.; Hunter, A. D.; Gray, T. G. *Proc. Natl. Acad. Sci., U.S.A.* **2008**, *105*, 14293–14297.

Scheme 3. Configuration Interaction in the Absorption Spectra of Azadipyrromethene Complexes Depicted for the Parent BF_2^+ Complex (C_{2v})[a]

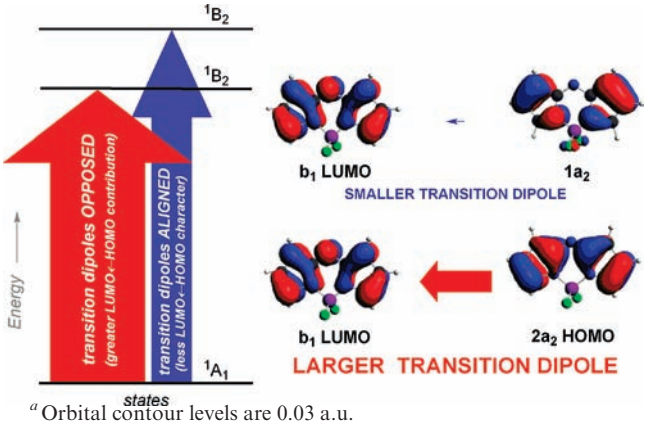

[a] Orbital contour levels are 0.03 a.u.

LUMO←HOMO and LUMO←HOMO − 1 transitions, or in the notation of Scheme 3, b_1←$2a_2$ and b_1←$1a_2$. The singlet states so derived are both B_2, and they engage in configuration interaction. The b_1←$2a_2$ (LUMO←HOMO) excitation carries a larger transition moment than the b_1←$1a_2$ (LUMO←HOMO − 1) promotion. For unsubstituted **10**, the two transitions contribute roughly equally to both absorptions. In the lower-energy state, the transition dipole vectors are opposed.

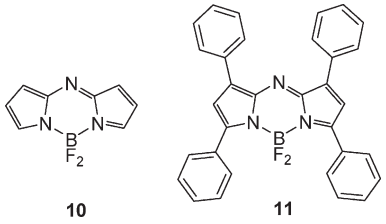

10 **11**

Time-dependent calculations of tetraphenyl azadipyrromethene ($\mathbf{L_a}$) complexes find that analogous transitions dominate the intense absorption calculated at 601 nm. As with **10**, transition dipole vectors for excitation to the lowest singlet excited state of $(H_3P)Cu\mathbf{L_a}$ *oppose* each other, with a 168° angle between them. However, the b_1←$2a_2$ (LUMO←HOMO) component carries a greater transition dipole moment than its higher-energy CI counterpart b_1←$1a_2$ (here, LUMO←HOMO − 3). So much greater is the norm of the LUMO←HOMO transition dipole vector that it predominates, and the 601 nm transition, primarily LUMO←HOMO, is more intense. Its companion transition, at 538 nm, is mainly b_1←$1a_2$, and the dipole contribution from b_1←$2a_2$ is augmentative. Transition dipole vectors for the 538-nm excitation lie at 11.6° to each other in $PH_3Cu\mathbf{L_a}$. However, the smaller b_1←$1a_2$ dipole vector leaves this additive transition with a lesser oscillator strength. Thus, an intense transition is calculated at 601 nm for $PH_3Cu\mathbf{L_a}$ with a minor absorption at 538 nm, corresponding to the b_1←$2a_2$ and b_1←$1a_2$ excitations of Scheme 3. Calculations for $PH_3Ag\mathbf{L_a}$ and for BF_2-azadipyrromethene **11** are broadly similar. Absorption profiles of azadipyrromethene fluorophores within the phototherapeutic window (ca. 600−900 nm) are determined by constitutive transition dipole moments, and not by relative weights in configuration interaction.

Conclusions

Syntheses and characterizations of three-coordinate azadipyrromethene complexes with group 11 metals are described. The copper(I) and silver(I) compounds are prepared by room temperature reactions of free azadipyrromethene ligands with (phosphine)metal(I) triflates in the presence of an amine base. We find that the synthetic methods described here are quite general, allowing for methoxy-substituted tetraarylazadipyrromethene complexes to be prepared, and permitting the facile substitution of triethylphosphine for triphenylphosphine. Ligand ^{1}H NMR resonances are generally unresponsive to metal complexation, though resonances associated with the proximal aryl rings do shift upfield by more than 0.3 ppm when PPh_3 occupies the third coordination site. NMR methods, in combination with combustion analysis, have established the purity of all new compounds, which are isolated in 65% or better yields. The structural features of the new complexes described here recall previously reported complexes. All complexes are tricoordinate with slight asymmetries in M−N bond lengths. The N−M−N coordination plane is canted relative to the mean plane of the ligand chromophore, and this canting is not relieved upon substitution of less sterically demanding PEt_3 for PPh_3. Also, both intra- and intermolecular π-stacking interactions, involving PPh_3 and pendant azadipyrromethene phenyls, are frequently observed in the solid state. ^{1}H NMR spectra suggest that these interactions persist in solution as well. All metal complexes described retain intense electronic absorption features in the red region of the visible spectrum, and weak red emission occurs. Methoxy-substituted azadipyrromethene complexes demonstrate red-shifted absorption and emission maxima relative to unsubstituted complexes, which mirrors the trend observed for previously characterized BF_2^+ and Zn(II) complexes.[44,45,60] At 77 K, the resolution of absorption and emission spectra is markedly improved, allowing for the discernment of at least three distinct absorption bands in the red region, and regular structure in the emission spectra.[62] The optical spectra suggest ligand-based electronic transitions, which time-dependent DFT calculations corroborate.

The experiments herein, along with our earlier report[60] of group 12 bis(azadipyrromethenes), and O'Shea and collaborators' disclosure[61] of first-row transition element azadipyrromethene complexes attest that these ligands are versatile. The visible absorption of azadipyrromethene ligands has for some years[44] commended their boron complexes for photodynamic therapy. The distinctive optical profiles of azadipyrromethenes persist upon complexing main group[60] and d-block metal centers.[61] Calculations described here show that the visible and near-ultraviolet photophysics of group 11 azadipyrromethenes are ligand-centered. The absorption properties are reminiscent of porphyrin electronic spectra in that two one-electron promotions to states of the same symmetry mingle through configuration interaction. The chelated Lewis acid minimally influences absorption or emission maxima. Optical transitions are more sensitive to methoxy substitution of the proximal ($\mathbf{L_b}$ series) or distal ($\mathbf{L_c}$ series) phenyl substituents. This sensitivity results from frontier orbital amplitude at the *para*-carbon atoms of all four benzene rings.

Investigations of phototherapy and cellular labeling with azadipyrromethene sensitizers will doubtless continue, but emerging ideas in medicinal chemistry pose new opportunities. Azadipyrromethene complexes of paramagnets such as gadolinium(III), or of radionuclides such as ^{99m}Tc or ^{111}In hold potential as dual-mode optical/MRI or optical/radioimaging agents, respectively. Their clinical applications, if any, lie in the future, but exciting discoveries with azadipyrromethenes are surely at hand.

Experimental Section

General Procedures. Triphenylphosphine (PPh_3), triethylphosphine (PEt_3), AgOTf (OTf = trifluoromethanesulfonate), diisopropylethylamine (DIPEA), and $(CuOTf)_2\cdot$toluene were obtained commercially and used as received. PPh_3AgOTf[87] and tetraarylazadipyrromethene ligands $\mathbf{L_{a\text{-}c}}$ were prepared as previously described.[45] The syntheses of **1**, **4**, and **9** were described earlier.[62] Air-sensitive solids were handled in an inert-atmosphere glovebox operating at < 10 ppm O_2. Reactions involving air-sensitive materials were carried out under an atmosphere of Argon using standard Schlenk-line techniques; solvents for such reactions were purified with an M-Braun SPS and purged with argon prior to use. ^{1}H and ^{31}P NMR spectra were recorded on a Varian AS-400 spectrometer, operating at 400 and 161.8 MHz, respectively. Microanalyses were performed by Quantitative Technologies Inc. and Robertson Microlit Laboratories. Absorption and corrected emission spectra were recorded in HPLC-grade chloroform on a Cary 5G spectrophotometer and a Cary Eclipse fluorimeter, respectively. Fluorescence quantum yields were determined using deoxygenated, optically dilute solutions with absorbance <0.1 at the respective excitation wavelength. $(Bu_4N)_2Mo_6Cl_{14}$ was used as a standard with a literature value for Φ_f of 0.19.[88]

PPh_3CuL_b (2). PPh_3CuOTf was generated *in situ* by stirring $(CuOTF)_2\cdot$toluene (26 mg, 0.050 mmol) and PPh_3 (27 mg, 0.10 mmol) in 5 mL of THF for 20 min at room temperature. To the resulting solution was added a solution of $\mathbf{L_b}$ (53 mg, 0.10 mmol) in 7 mL of THF via syringe, followed by DIPEA (0.16 mL, 0.98 mmol). The reaction mixture was stirred at room temperature for 1 h, at which time all volatiles were removed *in vacuo*. The resulting residue was dried *in vacuo* overnight to give a bluish-black solid, which was taken up in about 4 mL of toluene, filtered through Celite, and crystallized by vapor diffusion of pentane in a nitrogen glovebox. Yield: 66 mg (76%). ^{1}H NMR ($CDCl_3$): δ 8.04 (d, 4H), 7.88 (d, 4H), 7.26−7.39 (m, 9H), 7.15−7.19 (m, 8H), 6.93 (t, 6H), 6.42 (d, 4H), 3.60 (s, 6H). ^{31}P NMR ($CDCl_3$): δ 3.5 (s, br) ppm. UV−vis ($CHCl_3$): λ (ε) 320 (24000), 620 (28000) nm. Emission ($CHCl_3$, λ_{ex} = 550 nm): λ 665 nm. Anal. Calcd for $C_{52}H_{41}N_3O_2PCu$: C, 74.85; H, 4.95; N, 5.04. Found: C, 74.61; H, 4.69; N, 4.82.

PPh_3CuL_c (3). Prepared in the same manner as for **2**, using 25 mg (0.048 mmol) of $(CuOTF)_2\cdot$toluene, 25 mg (0.095 mmol) of PPh_3, and 49 mg (0.096 mmol) of $\mathbf{L_c}$; all other conditions identical to above. Yield: 63 mg (79%). ^{1}H NMR ($CDCl_3$): δ 8.01 (d, 4H), 7.91 (d, 4H), 7.26 (t, 3H), 7.11−7.15 (m, 8H), 6.83−6.98 (m, 16H), 3.89 (s, 6H). ^{31}P NMR ($CDCl_3$): δ 3.5 (s, br) ppm. UV−vis ($CHCl_3$): λ (ε) 306 (32000), 606 (38000) nm. Emission ($CHCl_3$, λ_{ex} = 550 nm): λ, 667, 705(sh) nm. Anal. Calcd for $C_{52}H_{41}N_3O_2PCu$: C, 74.85; H, 4.95; N, 5.04. Found: C, 74.73; H, 4.85; N, 4.88.

PPh_3AgL_b (5). PPh_3AgOTf (51 mg, 0.098 mmol) and $\mathbf{L_b}$ (50 mg, 0.098 mmol) were dissolved in 12 mL of THF, and DIPEA (0.16 mL, 0.98 mmol) was added via syringe. After stirring for 1 h at room temperature, the solvent was stripped via rotary evaporation. The resulting residue was taken up in 20 mL of benzene, and washed with 2×20 mL of H_2O. The organic layer was dried with $MgSO_4$ and evaporated to dryness. The product was crystallized from a concentrated THF solution via room temperature vapor diffusion of pentane. Yield: 58 mg (67%). ^{1}H NMR ($CDCl_3$): δ 7.95−7.98 (m, 8H), 7.29−7.35 (m, 9H), 7.18−7.22 (m, 8H), 6.90−6.95 (m, 6H), 6.35 (d, 4H), 3.52 (s, 6H). ^{31}P NMR ($CDCl_3$): δ 15.2 (d, br) ppm. UV−vis ($CHCl_3$): λ (ε) 324 (30000), 631 (69000) nm. Emission ($CHCl_3$, λ_{ex} = 550 nm): λ 667 nm. Anal. Calcd for $C_{52}H_{41}N_3O_2PAg$: C, 71.07; H, 4.70; N, 4.78. Found: C, 70.53; H, 4.40; N, 4.66.

PPh_3AgL_c (6). Prepared in the same manner as for **5**, using 51 mg (0.098 mmol) of PPh_3AgOTf and 50 mg (0.098 mmol) of $\mathbf{L_c}$; all other conditions identical to above. Yield: 59 mg (68%). ^{1}H NMR ($CDCl_3$): δ 8.03 (dd, 4H), 7.94 (d, 4H), 7.32 (td, 3H), 7.16−7.20 (m, 8H), 6.83−6.92 (m, 16H), 3.88 (s, 6H). ^{31}P NMR ($CDCl_3$): δ 13.2 (s, br) ppm. UV−vis ($CHCl_3$): λ (ε) 304 (39000), 615 (64000) nm. Emission ($CHCl_3$, λ_{ex} = 550 nm): λ 660, 705 (sh). Anal. Calcd for $C_{52}H_{41}N_3O_2PAg$: C, 71.07; H, 4.70; N, 4.78. Found: C, 70.68; H, 4.31; N, 5.13.

PEt_3AgL_a (7). PEt_3AgOTf was generated *in situ* by stirring AgOTf (26 mg, 0.10 mmol) and PEt_3 (22 μL, 0.15 mmol) in 5 mL of THF at room temperature for 20 min. To the resulting colorless solution was added a solution of $\mathbf{L_a}$ (43 mg, 0.096 mmol) in 7 mL of THF via syringe. Finally, DIPEA (0.16 mL, 0.98 mmol) was added via syringe. After stirring for 1 h at room temperature, the solvent was removed via rotary evaporation. The resulting residue was taken up in 30 mL of benzene, and washed with 2×20 mL of H_2O. The organic layer was dried over $MgSO_4$ and evaporated to give a brown solid. The product was recrystallized from a concentrated THF solution by room temperature vapor diffusion of pentane. Yield: 42 mg (65%). ^{1}H NMR ($CDCl_3$): δ 8.03 (d, 4H), 7.96 (d, 4H) 7.30−7.45 (m, 12H), 7.19 (s, 2H), 1.05−1.13 (m, 6H), 0.63−0.71 (m, 9H). ^{31}P NMR ($CDCl_3$): δ 8.2 (s, br) ppm. UV−vis ($CHCl_3$): λ (ε) 304 (30000), 610 (42000) nm. Emission ($CHCl_3$, λ_{ex} = 550 nm): λ, 645 nm. Anal. Calcd for $C_{38}H_{37}N_3PAg$: C, 67.66; H, 5.53; N, 6.23. Found: C, 68.25; H, 5.53; N, 6.23.

PEt_3AgL_c (8). Prepared in same manner as for **7**, using 26 mg (0.10 mmol) of AgOTf, 22 μL (0.15 mmol) of PEt_3, and 49 mg (0.096 mmol) of $\mathbf{L_c}$; all other conditions identical to above. Yield: 49 mg (69%). ^{1}H NMR ($CDCl_3$): δ 8.02 (d, 4H), 7.93 (d, 4H), 7.33−7.44 (m, 6H), 7.11 (s, 2H), 6.90 (d, 4H), 3.87 (s, 6H), 1.05−1.11 (m, 6H), 0.62−0.70 (m, 9H). ^{31}P NMR ($CDCl_3$): δ 8.8 (d, br) ppm. UV−vis ($CHCl_3$): λ (ε) 303 (31000), 614 (46000) nm. Emission ($CHCl_3$, λ_{ex} = 550 nm): λ 661, 702 (sh) nm. Anal. Calcd For $C_{40}H_{41}N_3O_2PAg$: C, 65.40; H, 5.62; N, 5.72. Found: C, 66.03; H, 5.69; N, 5.73 .

X-ray Structure Determination. Products were crystallized by diffusion of pentane into saturated toluene or THF solutions. Single crystal X-ray data were collected on a Bruker AXS SMART APEX CCD diffractometer using monochromatic Mo Kα radiation with omega scan technique. The unit cells were determined using SMART[89] and SAINT+.[90] Data collection for all crystals was conducted at 100 K (−173 °C). All structures were solved by direct methods and refined by full matrix least-squares against F^2 with all reflections using SHELXTL.[91] Refinement of extinction coefficients was found to be insignificant. All non-hydrogen atoms were refined anisotropically. All hydrogen atoms were placed in standard calculated positions and all hydrogen atoms were refined with an

(87) Lettko, L.; Wood, J. S.; Rausch, M. D. *Inorg. Chim. Acta* **2000**, *308*, 37–44.

(88) Maverick, A. W.; Najdzionek, J. S.; MacKenzie, D.; Nocera, D. G.; Gray, H. B. *J. Am. Chem. Soc.* **1983**, *105*, 1878–1882.

(89) *Bruker Advanced X-ray Solutions, SMART for WNT/2000* (*Version 5.628*), Bruker AXS Inc., Madison, WI: USA, 1997−2002.

(90) *Bruker Advanced X-ray Solutions, SAINT*, Version 6.45; Bruker AXS Inc.: Madison, WI, 1997−2003.

(91) *Bruker Advanced X-ray Solutions, SHELXTL*, Version 6.10; Bruker AXS Inc.: Madison, WI, 2000.

isotropic displacement parameter 1.2 times that of the adjacent carbon.

Computations. Scalar-relativistic DFT calculations were executed within the zero-order regular approximation, as implemented in the Amsterdam Density Functional package (ADF2006).[92−94] All calculations were spin-restricted. In these computations, the local density functional is that of Vosko, Wilk, and Nusair.[95] Gradient corrections were introduced with the exchange functional of Becke[96] and the correlation functional of Perdew.[97,98] Scalar relativistic interactions were included within the zero-order regular approximation (ZORA).[99−102] Atomic orbitals of all atoms were constructed from triple-ζ basis sets of Slater orbitals (ADF database TZP). Core electronic shells (one or more principle quantum numbers below the valence level) were frozen for all atoms. The electron density was fitted with sets of auxiliary s, p, d, f, and g-functions centered on all nuclei, along with the Coulomb and exchange potentials, in every self-consistent field cycle. Gas-phase geometries were optimized with the Broyden−Fletcher−Goldfarb−Shano algorithm; the convergence criterion was that successive energies differ by not more than 1×10^{-4} H (the default is 1×10^{-3} H). Numerical harmonic frequency calculations verified that all converged structures are potential-energy minima. Vertical excitation energies were calculated with single-point time-dependent DFT calculations,[103−105] performed with the asymptotically correct LB94 functional of van Leeuwen and Baerends[106] or the statistical average of model exchange-correlation potentials (SAOP)[107] at the geometry previously optimized with the Becke−Perdew functional. Basis sets for time-dependent calculations are those used in geometry optimization. Time-dependent calculations employed the Davidson algorithm; error tolerances in the square of the excitation energies and the trial-vector orthonormality cutoff were both set to 10^{-8}. Time-dependent calculations employed the conductor-like screening model of Klamt and co-workers (COSMO) using chloroform solvent,[80−82] in single-point calculations on the gas-phase structures.

Acknowledgment. The authors thank the National Science Foundation (Grant CHE-0749086 to T.G.G.). T.G.G. is an Alfred P. Sloan Research Fellow. T.S.T. acknowledges the Case Western Reserve University SOURCE program for funding; he currently holds a John and Fannie Hertz Foundation predoctoral fellowship. The diffractometer at Case Western Reserve was funded by NSF Grant CHE-0541766. We thank Professor D. G. Nocera, Massachusetts Institute of Technology, for access to instrumentation, and Dr. D. V. Partyka for experimental assistance.

Supporting Information Available: X-ray crystallographic data in CIF format, optical absorption and emission spectra for ligands $\mathbf{L_{a-c}}$ and complexes **1**−**9**. This material is available free of charge via the Internet at http://pubs.acs.org.

(92) *SCM* ; Theoretical Chemistry, Vrije Universiteit: Amsterdam, The Netherlands, http://www.scm.com.
(93) te Velde, G.; Bickelhaupt, F. M.; Baerends, E. J.; Guerra, F. C.; van Gisbergen, S. J. A.; Snijders, J. G.; Ziegler, T. *J. Comput. Chem.* **2001**, *22*, 931–967.
(94) Guerra, F. C.; Visser, O.; Snijders, J. G.; te Velde, G.; Baerends, E. J. In *Methods and Techniques for Computational Chemistry*; Clementi, E., Corongiu, C., Eds.; STEF: Cagliari, 1995; pp 303−395.
(95) Vosko, S. H.; Wilk, L.; Nusair, M. *Can. J. Phys.* **1980**, *58*, 1200–1211.
(96) Becke, A. D. *Phys. Rev. A* **1988**, *38*, 3098–3100.
(97) Perdew, J. P.; Zunger, A. *Phys. Rev. B* **1981**, *23*, 5048–5079.
(98) Perdew, J. P. *Phys. Rev. B* **1986**, *33*, 8822–8824.
(99) Van Lenthe, E.; Baerends, E. J.; Snijders, J. G. *J. Chem. Phys.* **1993**, *99*, 4597–4610.
(100) Van Lenthe, E.; Baerends, E. J.; Snijders, J. G. *J. Chem. Phys.* **1994**, *101*, 9783–9792.
(101) Van Lenthe, E.; Snijders, J. G.; Baerends, E. J. *J. Chem. Phys.* **1996**, *105*, 6505–6516.
(102) Van Lenthe, E.; van Leeuwen, R.; Baerends, E. J.; Snijders, J. G. *Int. J. Quantum Chem.* **1996**, *57*, 281–293.
(103) van Gisbergen, S. J. A.; Kootstra, F.; Schipper, P. R. T.; Gritsenko, O. V.; Snijders, J. G.; Baerends, E. J. *Phys. Rev. A* **1998**, *57*, 2556–2571.
(104) Jamorski, C.; Casida, M. E.; Salahub, D. R. *J. Chem. Phys.* **1996**, *104*, 5134–5147.
(105) Bauernschmitt, R.; Ahlrichs, R. *Chem. Phys. Lett.* **1996**, *256*, 454–464.
(106) van Leeuwen, R.; Baerends, E. J. *Phys. Rev. A* **1994**, *49*, 2421–2431.
(107) Schipper, P. R. T.; Gritsenko, O. V.; van Gisbergen, S. J. A.; Baerends, E. J. *J. Chem. Phys.* **2000**, *112*, 1344–1352.